

# A potent protective bispecific nanobody targeting Herpes simplex virus gD reveals vulnerable epitope for neutralizing

Received: 18 August 2024

Accepted: 28 March 2025

Published online: 06 May 2025

 Check for updates

Jing Hu<sup>1,12</sup>, Haoyuan Tan<sup>2,12</sup>, Meihua Wang<sup>3</sup>, Shasha Deng<sup>3</sup>, Mengyao Liu<sup>3</sup>, Peiyi Zheng<sup>3</sup>, Anmin Wang<sup>2</sup>, Meng Guo<sup>2</sup>, Jin Wang<sup>3</sup>, Jiayin Li<sup>3</sup>, Huanwen Qiu<sup>3</sup>, Chengbing Yao<sup>4</sup>, Zhongliang Zhu<sup>3,4</sup>, Chaolu Hasi<sup>5</sup>, Dongli Pan<sup>6</sup>, Hongliang He<sup>1</sup>, Chenghao Huang<sup>7</sup>, Yuhua Shang<sup>4</sup>, Shu Zhu<sup>2,8</sup> ✉ & Tengchuan Jin<sup>1,2,3,4,8,9,10,11</sup> ✉

Herpes simplex virus (HSV) causes significant health burden worldwide. Currently used antiviral drugs are effective but resistance can occur. Here, we report two high-affinity neutralizing nanobodies, namely Nb14 and Nb32, that target non-overlapping epitopes in HSV gD. Nb14 binds a neutralization epitope located in the N-A' interloop, which prevents the interaction between gD and gH/gL during the second step of conformational changes during membrane fusion after virus attachment. The bispecific nanobody dimer (Nb14-32-Fc) exhibits high potency in vitro and in vivo. Mechanistically, Nb14-32-Fc neutralizes HSVs at both the pre- and post-attachment stages and prevents cell-to-cell spread in vitro. Administration of Nb14-32-Fc at low dosage of 1 mg/kg provides 100% protection in an HSV-1 infection male mouse model and an HSV-2 infection female mouse model. Our results demonstrate that Nb14-32-Fc could serve as a promising drug candidate for treatment of HSV infection, especially in the cases of antiviral drug resistance and severe herpes encephalitis.

Herpes simplex virus (HSV) is a  $\alpha$ -herpesvirus that can infect the humans of all ages for their life time<sup>1</sup>. Two serotypes of HSV, HSV-1 and HSV-2 can cause different symptoms. HSV-1 mainly causes mucosal diseases, including orofacial infections, conjunctivitis, keratitis and

encephalitis, while HSV-2 infection is one of the most prevalent sexually transmitted infections that mainly causes recurrent genital herpes<sup>2–5</sup>. The World Health Organization (WHO) in 2016 reported that >3.7 billion people aged 0–49 years are infected with oral herpes

<sup>1</sup>Department of Infectious Diseases, The First Affiliated Hospital of USTC, Division of Life Sciences and Medicine, Center for Advanced Interdisciplinary Science and Biomedicine of IHM, University of Science and Technology of China, Hefei, Anhui 230001, P.R. China. <sup>2</sup>National Key Laboratory of immune response and immunotherapy, School of Basic Medical Sciences, Division of Life Sciences and Medicine, University of Science and Technology of China, Hefei 230027, China. <sup>3</sup>Laboratory of Structural Immunology, National Key Laboratory of Immune Response and Immunotherapy, Division of Life Sciences and Medicine, University of Science and Technology of China, Hefei 230027, China. <sup>4</sup>Anhui Genebiol Biotech. LTD, Hefei 230000, China. <sup>5</sup>Sonid Suoqi Animal Husbandry Workstation, Xilinhot City, Inner Mongolia Xilin Gol League, Xilinhot, China. <sup>6</sup>Department of Medical Microbiology and Parasitology, Zhejiang University School of Medicine, Hangzhou, Zhejiang, China. <sup>7</sup>State Key Laboratory of Vaccines for Infectious Diseases, National Institute of Diagnostics and Vaccine Development in Infectious Diseases, Xiang An Biomedicine Laboratory, Department of Laboratory Medicine, School of Public Health, Xiamen University, Xiamen 361102, China. <sup>8</sup>Institute of Health and Medicine, Hefei Comprehensive National Science Center, Hefei, Anhui, China. <sup>9</sup>Key Laboratory of Anhui Province for Emerging and Reemerging Infectious Diseases, Hefei 230027, China. <sup>10</sup>Biomedical Sciences and Health Laboratory of Anhui Province, University of Science & Technology of China, Hefei 230027, China. <sup>11</sup>Clinical Research Hospital of Chinese Academy of Sciences (Hefei), University of Science and Technology of China, Hefei 230001, China. <sup>12</sup>These authors contributed equally: Jing Hu, Haoyuan Tan. ✉ e-mail: [zhushu@ustc.edu.cn](mailto:zhushu@ustc.edu.cn); [jint@ustc.edu.cn](mailto:jint@ustc.edu.cn)

worldwide, and about 500 million people aged 15–49 have genital herpes globally<sup>6</sup>. Moreover, neonatal herpes simplex virus (nHSV) infection has the highest infant mortality rate among perinatal viral infections<sup>7,8</sup>. HSV-2 infection also further increases the risk of HIV acquisition<sup>9,10</sup>.

Acyclovir, famciclovir, and valacyclovir are relatively safe and efficacious viral DNA-targeted agents that are currently available for the treatment of primary genital herpes<sup>11–13</sup>. However, a series of problems remain to be solved, such as insufficient efficacy, low safety, drug resistance, and so on<sup>14</sup>. At the same time, small molecule drugs cannot completely eradicate the latent virus in the ganglia, resulting in lifetime and repeated infections<sup>15</sup>. Antiviral antibodies with distinct mechanisms from small molecule antivirals are promising approach against HSV. To date, a few monoclonal antibodies (mAbs), such as HSV8, CH42 and CH43, E317, and hu2c, have shown therapeutic efficacy against HSV infection in animal models<sup>16–19</sup>. Nonetheless, no single antibody is currently used for the treatment of HSV infection in the clinic. Neutralizing mAbs exert neutralizing activity by targeting glycoproteins that mediate binding to receptors or influence membrane fusion<sup>20</sup>. gD is the most abundantly expressed glycoprotein on the virions and acts as the receptor-binding protein crucial for facilitating the fusion and entry of HSV into host cells, stimulating virus-neutralizing antibodies production in human after HSV infection<sup>21,22</sup>. Therefore, gD has been the predominant candidate for HSV therapeutic antibody<sup>23</sup>.

Camelid-derived VHH antibodies, also known as nanobodies (Nbs), are natural, single-heavy-chain monovalent antibody fragments<sup>24</sup>. Nbs are easier to produce in different expression systems with higher thermal stability and solubility, and thus are superior to conventional antibodies in storage and transportation. Moreover, nanobodies consist of only one Ig domain and thus are easier to engineer into multivalent formats than conventional antibodies<sup>25,26</sup>. Multivalent engineering, including artificial homo- and heteromultivalences is an effective approach that significantly enhances overall avidity as well as neutralization potency, such strategy has been successfully used in SARS-CoV-2 neutralization Ab development<sup>26,27</sup>.

In this study, we aim to use nanobodies to probe novel and conserved neutralization epitopes for HSV gD and design therapeutic antibodies for the treatment of HSV infection and diseases.

## Results

### Identification of two neutralizing nanobodies (Nb14 and Nb32) targeting different epitopes in HSV gD

To obtain HSV-2 gD-specific neutralizing nanobodies, a camel was immunized with recombinant HSV-2 gD and a phage library displaying all VHHs was constructed. After two rounds of panning, 13 nanobody colonies positive for HSV-2 gD were selected and expressed as Nb-Fc fusion in HEK293F cells to improve the efficacy (Fig. 1a, b). The neutralizing activities of these Nb-Fc homodimers were preliminarily evaluated by flow cytometry using modified HSV-1-GFP (Fig. 1c). The neutralizing antibodies can inhibit the virus from infecting the cell, which is manifested as reduced fluorescence. Among them, Nb14-Fc and Nb32-Fc effectively inhibit HSV-1 infection with >90% inhibition at 1 µg/mL while the remaining 11 nanobodies showed no obvious inhibitory activity with <60% inhibition (Fig. 1d). Following the initial functional evaluation, the binding kinetics of Nb14-Fc and Nb32-Fc to HSV gD proteins were further characterized via the ELISA and the Surface plasma resonance (SPR) assays (Fig. 2a–f). The effective concentration ( $EC_{50}$ ) revealed by ELISA for HSV-1 gD interacted with Nb14 and Nb32 are 0.04 nM and 0.09 nM, respectively. Similarly, the  $EC_{50}$  values of HSV-2 gD interacted with Nb14 and Nb32 are 0.04 nM and 0.10 nM (Fig. 2a, b). The kinetic binding analysis by SPR also revealed that Nb14-Fc and Nb32-Fc tightly bound to the HSV-1/HSV-2 gD with equilibrium dissociation constant ( $K_D$ ) values of 1.14 nM/83.10 pM and 36.70/43.40 pM,

respectively (Fig. 2c–f). Benefiting from the high-affinity HSV gD binding, both Nb14-Fc and Nb32-Fc potently neutralized HSV-1 and HSV-2 viruses in a dose-dependent manner in the in vitro neutralization assay with or without any complement components (Fig. S2). Nb32-Fc exhibited higher potency against HSV-1/2, with an  $IC_{50}$  of 0.51/0.50 nM, than that of Nb14, with  $IC_{50}$  of 8.54/59.28 nM in the absence of complement components (Fig. 2g, h). In parallel, we evaluated whether Nb14 and Nb32 could simultaneously bind to HSV gD via the competitive ELISA. The Nb32 were serially diluted and used to compete with 5 nM of Nb14-Fc solutions to bind HSV-2 gD coated on plates. The results revealed that the increased concentration of Nb32 did not inhibit the binding of Nb14-Fc (Fig. 2i), indicating that the two nanobodies target on non-overlapping epitopes on the HSV gD antigen.

### Structural basis for the neutralization by Nb14 and Nb32

To elucidate the structural basis by which Nb14 recognizes the HSV gD, we solved the crystal structure of the nanobody bound to HSV-2 gD at a resolution of 3.7 Å. The structure was determined by molecular replacement method and refined to  $R_{work}$  = 0.301 and  $R_{free}$  = 0.347, respectively (Table S1). Each crystallographic asymmetric unit contained a single Nb14/HSV-2 gD complex bound in a 1:1 binding mode. Overall, Nb14 mainly utilizes its long CDR3 to interact with a conformational epitope located on the external loop between the N terminal and the A' β-sheet of gD (the N-A' interloop) (Fig. 3a). Detailed analysis of the Nb14/HSV-2 gD interactions revealed an extended interface involved Nb14 residues F99, R117 and R119 in CDR3, R45 in the framework region and HSV-2 gD residues P47, Q49, I55 and D104 and N105 in the external loop (Fig. 3b). Among engagements formed by these residues, a total of thirteen hydrophilic interactions (five hydrogen bonds and eight salt bridges) were observed, stabilizing the Nb14/HSV-2 gD complex to some extent. Superimposed with the known HSV-1 gD structure, it is found that when D104 becomes G104 that lacks a side chain, there will be no salt bridge between HSV-1 gD and Nb14, and the interaction force will decrease, which may be the reason why the Nb14 has a higher affinity toward HSV-2 gD (Fig. 2c, e, Fig. S5). In addition, we further found that binding epitopes of Nb14 do not overlap with that of both known receptors, including HVEM and Nectin-1. The HVEM binding sites of gD are confined to A7-N15 and V24-P32 in the N-terminal hairpin domain<sup>28</sup>. The Nectin-1 binding sites of gD congregate into two main surface patches. P23, L25 to Q27, F223, N227, V231, and Y234 form the patch1, and patch2 residues includes R36 to H39, Q132, R134, V214 to R222<sup>29–31</sup>. Both receptors share an overlapping epitope. All reported antibodies bind close to the receptor binding domain, while Nb14 binds at the N-A' interloop far from the receptor binding domain, suggesting it is a novel antibody neutralization epitope (Fig. 3e, f).

In parallel with the determination of Nb14/HSV-2 gD structure, we also collected a 2.9 Å resolution data set from Nb32/HSV-2 gD crystals. The solved complex structure, with an  $R_{work}$  of 0.216 and an  $R_{free}$  of 0.276 (Table S1), includes two Nb32/HSV-2 gD complex molecules bound in a 1:1 binding mode per asymmetric unit. Overall, Nb32 targeted to a conformational epitope located on the upper sheet region and a small portion of loops of HSV-2 gD (Fig. 3c). Detailed analyses revealed that the epitope was composed of HSV-2 gD residues K35, R36, Y38–I40, T116 and D215 and that the Nb32 residues Y32, Y52, S56 and Y105–Y108. These amino acids formed an extended interaction network, featuring with eight hydrogen bonds (Fig. 3d). Intriguingly, the residues Y38, H39 and D215 are critical amino acids involved in the binding of Nectin-1 to HSV gD. Alignment of the Nb32/HSV-2 gD and the Nectin-1/HSV-2 gD structures clearly showed that the Nb32 sterically clashed with the bound Nectin-1 and partially coincides with the reported E317 antibody epitope, indicating that Nb32 may directly block the binding of HSV

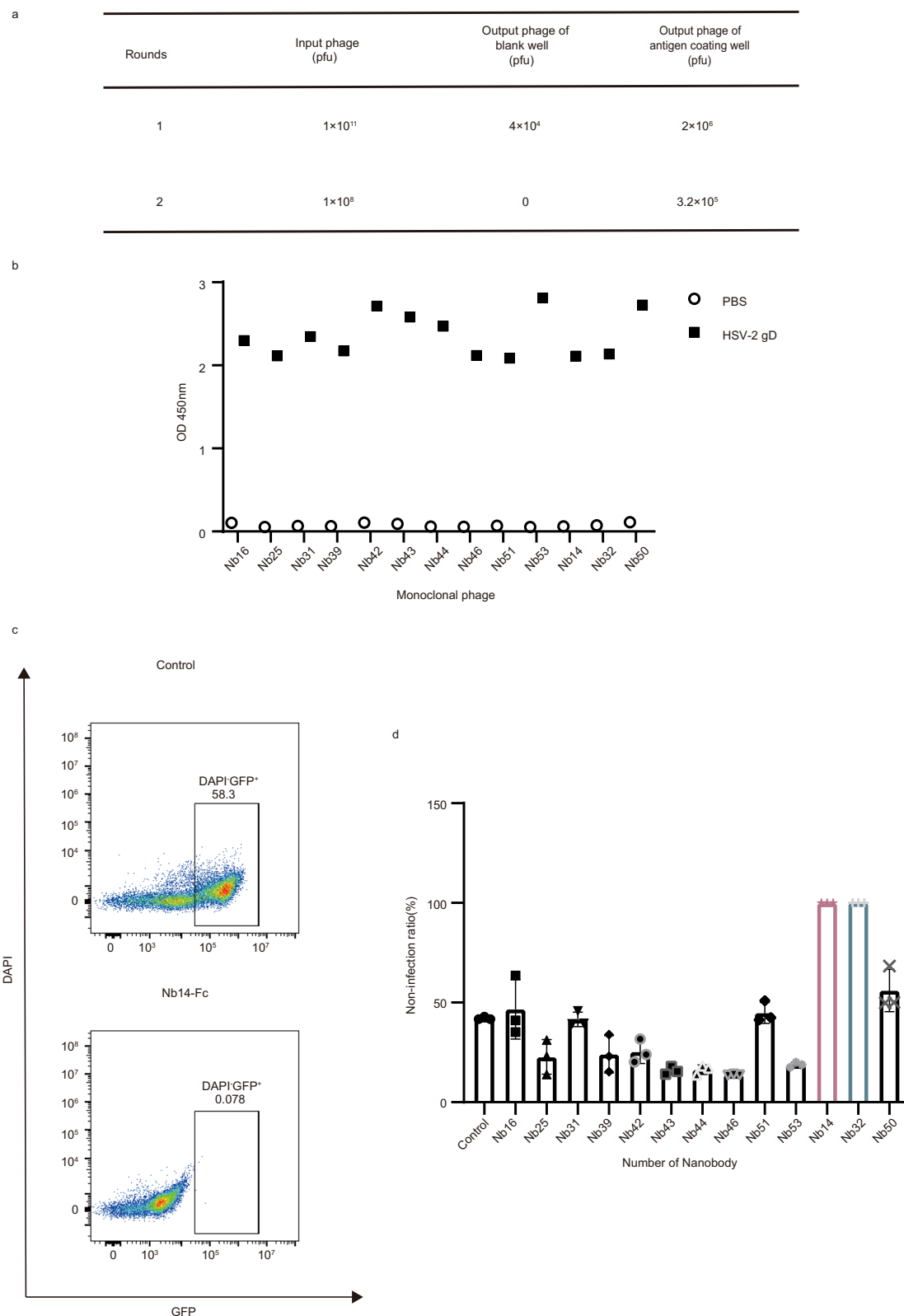
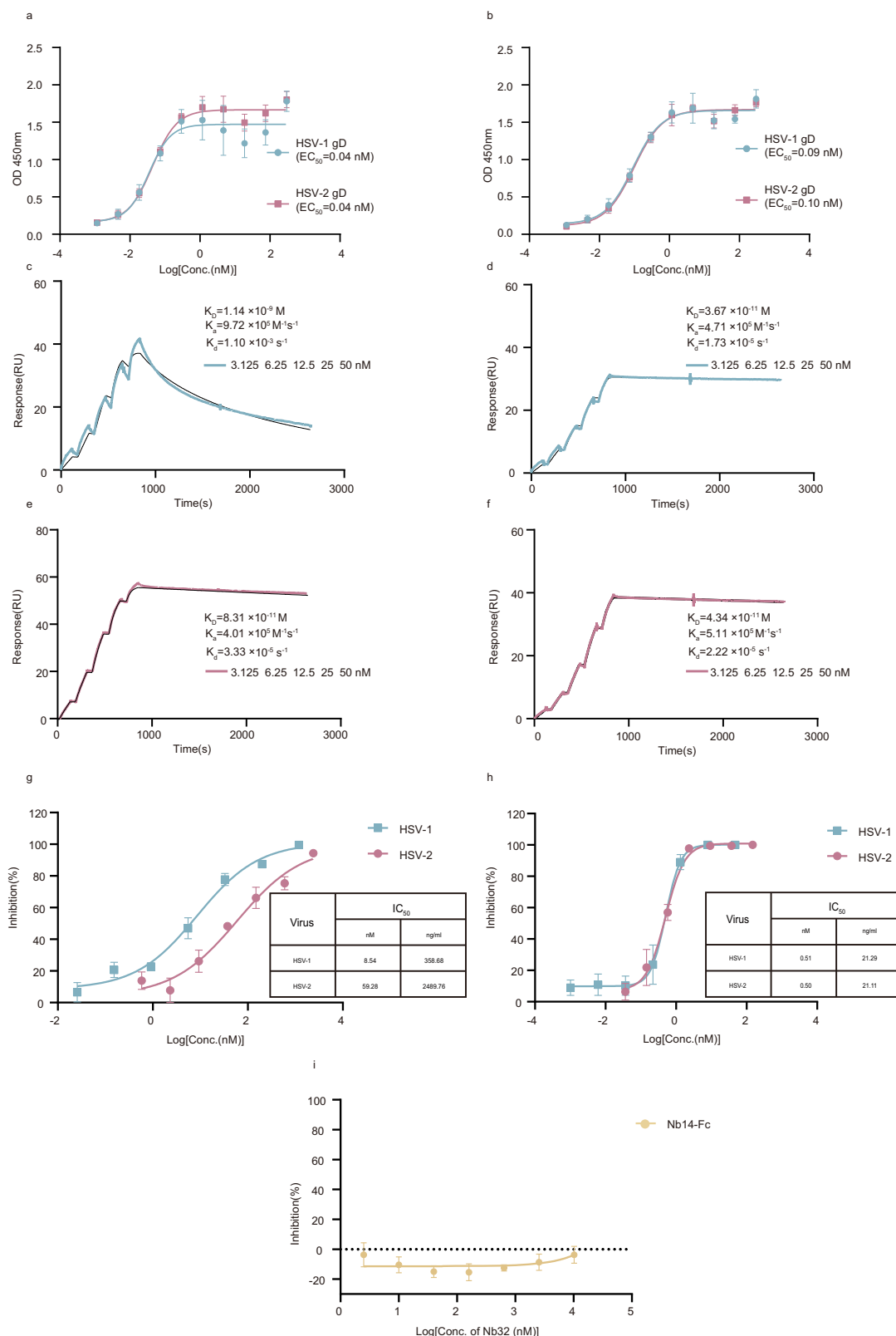


### Fig. 1 | Isolation and preliminary screening of anti-HSV-2 gD nanobodies.

**a** Enrichment of phages after panning on HSV-2 gD. **b** Monoclonal phage ELISA results for characterizing the binding of the isolated Nbs to HSV-2 gD. Each point represents a nanobody single colony. PBS group was used as a negative control. **c, d** Thirteen nanobodies ( $n = 13$ ) at  $1 \mu\text{g}/\text{mL}$  were tested for neutralization effects against HSV-1-GFP by flow cytometry. The intensity of fluorescence reflects the

neutralization activity of antibody. **c** Representative images of Nb14-Fc group and control group (Fc alone). **d** Non-infection ratio of thirteen nanobodies. Nb14-Fc and Nb32-Fc could inhibit  $> 90\%$  HSV-1 infection. Data and error bars are mean  $\pm$  S.D,  $n = 3$  biological independent experiments. Source data are provided as a Source Data file.



gD to receptor Nectin-1 for neutralization (Fig. 3f). When compared with the contact binding surface of E317, which covers an area of 1010 Å<sup>2</sup>, the binding surface of Nb32 covers only 583 Å<sup>2</sup>. This highlights the ability of Nb32 to achieve high binding affinities across a much smaller molecular footprint than conventional full-length immunoglobulins.

**Nb32 prevents the interaction between gD-Nectin-1 and Nb14 prevents the interaction between gD-gH/gL**

To further validate the competitive relationship between the antibodies and the two receptors observed in the structure, we further performed competitive binding experiments based on ELISA and SPR, respectively. In the former experiment, the CHO-K1 cells expressing

**Fig. 2 | Identification of two neutralizing nanobodies (Nb14-Fc and Nb32-Fc) targeting two different epitopes on HSV gD.** **a, b** Multi-concentration ELISA-binding assay of Nb14-Fc (**a**) and Nb32-Fc (**b**) towards HSV gD. The OD<sub>450</sub> emissions are depicted by curves. EC<sub>50</sub> (nM) indicated median effect concentration and was calculated to assess the binding potency of Nbs. **c, d** The binding kinetics of Nb14-Fc (**c**) and Nb32-Fc (**d**) to HSV-1 gD were monitored by the Biacore 8 K system. **e, f** The binding kinetics of Nb14-Fc (**e**) and Nb32-Fc (**f**) to HSV-2 gD were monitored by the Biacore 8 K system. The actual responses (colored lines) and the data fitted to a 1:1 binding model (black dotted lines) are shown in (**c–f**).  $K_D$ , equilibrium dissociation constant;  $k_a$ , association constant;  $k_d$ , dissociation constant. **g, h** The neutralizing activities of Nb14-Fc (**g**) and Nb32-Fc (**h**) against HSV-1 and HSV-2. The

half-maximal inhibitory concentration (IC<sub>50</sub>) values of the plaque reduction neutralization test (PRNT) were calculated by fitting the inhibition rates against antibody concentrations with a sigmoidal dose-response curve. **i** Competitive binding of Nb14-Fc and Nb32 to HSV-2 gD detected by ELISA. HSV-2 gD was coated on 96-well plates, Nb14-Fc was mixed with 4-fold serial dilutions of Nb32. The competition was determined by the reduction of the HRP-anti-IgG1 Fc induced chemiluminescence signal (OD<sub>450</sub>). The inhibition was calculated by comparing it to the Nb negative-control well. Data and error bars are mean ± S.D,  $n = 3$  biological independent experiments in (**a, b, and g–i**). Nb, Nanobody. Source data are provided as a Source Data file.

either receptor was coated to the plate and gD was preincubated with antibodies at varying concentrations before being added to the plate. In the latter, HSV-2 gD was immobilized on the CM5 chip and saturated antibodies were injected to gD firstly, followed by the injection of HVEM or Nectin-1 or original antibodies. As expected, the results of both experiments showed that Nb14-Fc did not affect the binding of either receptor to gD, while Nb32-Fc competitively bound gD with Nectin-1 (Fig. 4a–d). Meanwhile, we also conducted neutralization assay in CHO-K1 cells stably expressing only one receptor. Virus was incubated with antibodies firstly and then added to CHO-K1 cells, and the viral titers were detected by qPCR. The results of neutralization assay showed that Nb32 could effectively inhibit HSV infection in CHO-K1-Nectin-1 cells at concentration of 10 µg/ml, while Nb14 could effectively inhibit HSV infection in both CHO-K1-Nectin-1 cells and CHO-K1-HVEM cells at concentration of 50 µg/ml (Fig. 4e).

We also further explored the mechanisms of how Nb14 neutralized without blocking receptor binding by virus-free fusion assays. In brief, a mixture of gD-ZsGreen, gB-ZsGreen, gH/gL-ZsGreen plasmids were co-transfected into HEK293T cells. The cells were cultured in medium containing antibodies. 48 h post transfection, we observed significant inhibition of syncytium formation in the presence of antibodies. To evaluate fusion activity, we quantified the relative syncytial area and found that Nb14-Fc effectively inhibited viral glycoprotein mediated cell-to-cell fusion (Fig. 5a). Furthermore, in the luciferase reporting system, effector CHO cells were transfected with glycoprotein plasmids and pGL5-Luc reporter plasmids, and target HEK293T cells were transfected with pBind-Id and pACT-Myod plasmids additionally, the expression of pBind-Id and pACT-Myod significantly stimulated firefly luciferase expression in pGL5-Luc if fusion occurred. The results of the luciferase assay also showed that Nb14 could significantly inhibit cell fusion with low luciferase activity (Fig. 5b).

HSV-induced fusion consists of several sequential steps: (i) binding of gD to a receptor (Nectin-1 or HVEM), followed by (ii) a conformational change in gD that allows it to activate the regulatory protein gH/gL, leading to (iii) activation of gB into a fusogenic state<sup>32–34</sup>. Without interfering with the first step, we hypothesize that Nb14 may interfere with gD to activate gH/gL in the second step. Through cell-based binding and competition ELISA, we found that the gD can bind to the gH/gL expressed on the surface of CHO-K1 cells with EC<sub>50</sub> of 1.28 µM. However, pre-incubation of gD with Nb14 indeed partially inhibits the interaction between gD and gH/gL (Fig. 5c, d).

### A bispecific antibody Nb14-32-Fc effectively neutralizes HSV-1/2 at both the pre- and post-attachment stages and blocks cell-to-cell spread

To improve the neutralization efficacy and the mutation resistance, we fused Nb14-Fc to the C-terminus of Nb32 with five repeated Gly-Ser linkers to construct a novel bispecific Nb dimer, termed Nb14-32-Fc (Fig. 6a). Further SPR analysis showed that the binding affinity of Nb14-32-Fc to HSV-2 gD is almost 2-fold higher than that of the single Nb32-Fc (Fig. 2d, f), with  $K_D$  values of 38.10 pM to HSV-1 gD and 24.10 pM to HSV-2 gD, respectively (Fig. 6b). Consistent with the increased

affinities, Nb14-32-Fc exhibited almost 2-fold enhanced activity (on a molar basis) than Nb32-Fc alone in neutralizing HSV-2 (Figs. 2h, 6d). Nb14-32-Fc also showed a remarkable enhancement in neutralizing both HSVs compared to the E317 mAb (Fig. 6c, d), which is currently in clinical trials (NCT02346760, NCT03595995, NCT04714060, and NCT04979975)<sup>35</sup>. In the absence of complement components, the calculated IC<sub>50</sub> values of Nb14-32-Fc against HSV-1 and HSV-2 infection of cells in the in vitro plaque reduction and neutralization test (PRNT) assay were 0.39 nM and 0.22 nM, respectively. While for E317, the IC<sub>50</sub> value were 3.85 nM and 3.04 nM as revealed in a parallel assay (Fig. 6c, d).

To further explore the mode of neutralizing action of Nb14-32-Fc, we compared the in vitro neutralization efficacy of Nb14-32-Fc when the antibody was added to Vero cells before (pre-attachment) or after (post-attachment). PRNT results showed at pre- and post-attachment stage, HSV-1 and HSV-2 infection were nearly completely inhibited when using an Nb14-32-Fc concentration at 35.70 nM and 111.60 nM. Meanwhile, Nb14-32-Fc showed similar neutralizing IC<sub>50</sub> in the pre- and post-attachment assays, in which the IC<sub>50</sub> to HSV-1 were 0.46 nM and 0.39 nM, and the IC<sub>50</sub> to HSV-2 were 0.25 nM and 0.24 nM, respectively (Fig. 6e, f), which demonstrated Nb14-32-Fc could neutralize HSV infection at both the pre- and post-attachment stages with nearly equal efficiency.

Direct transmission between infected cells to uninfected adjacent cells (cell-to-cell spread) is an efficient and common route for HSV to evade immune surveillance<sup>36</sup>. Thus, the ability of blocking the cell-to-cell spread is considered to be a crucial aspect for evaluating the protective efficacy of neutralizing antibodies. To analyze the ability of Nb14-32-Fc and its parental Nbs in inhibiting cell-to-cell spread of HSV, an infectious center assay was utilized. In this assay infected cells were seeded on a monolayer of uninfected cells plated to 50%–60% percent confluence, prior to exposure to antibodies. The results illustrated that all four antibody-treated groups including positive control 4A3 effectively inhibited cell-cell spread, with Nb14-32-Fc showing the best inhibitory efficacy in which the HSV-1 and HSV-2 infected areas were -10% and 15% of the control group, respectively. In contrast, the infected areas in the Nb14-Fc, Nb32-Fc, and 4A3 treated groups ranged between 20%–60% of the control group (Fig. 6g, h). In parallel, HSV-1 transmission from infected GFP<sup>+</sup> cell to uninfected CellTracker Blue<sup>+</sup> cells was subsequently quantified by analyzing CellTracker Blue<sup>+</sup> GFP<sup>+</sup> populations with flow cytometry. The proportion of CellTracker Blue<sup>+</sup> GFP<sup>+</sup> Vero cells in Nb14-32-Fc treated sample was -1/10 of the control group, respectively (Fig. S1a). Similarly, Nb14-32-Fc produced uniformly small plaques that was about 1/3 the size of those of control group in the post absorption virus neutralization assay (Fig. S1b).

### Nb14-32-Fc protected mice against lethal HSV-1 intracranial infection

To evaluate the protective efficacy of neutralization antibodies against HSV-1 infection in vivo, we established a male C57BL/6j mouse intracranial infection model with lethal HSV-1 challenge. Nb14-Fc, Nb32-Fc, and Nb14-32-Fc were tested in parallel. The mice were infected with a lethal dose of HSV-1 viruses, and then, the mice were treated with 1 mg/



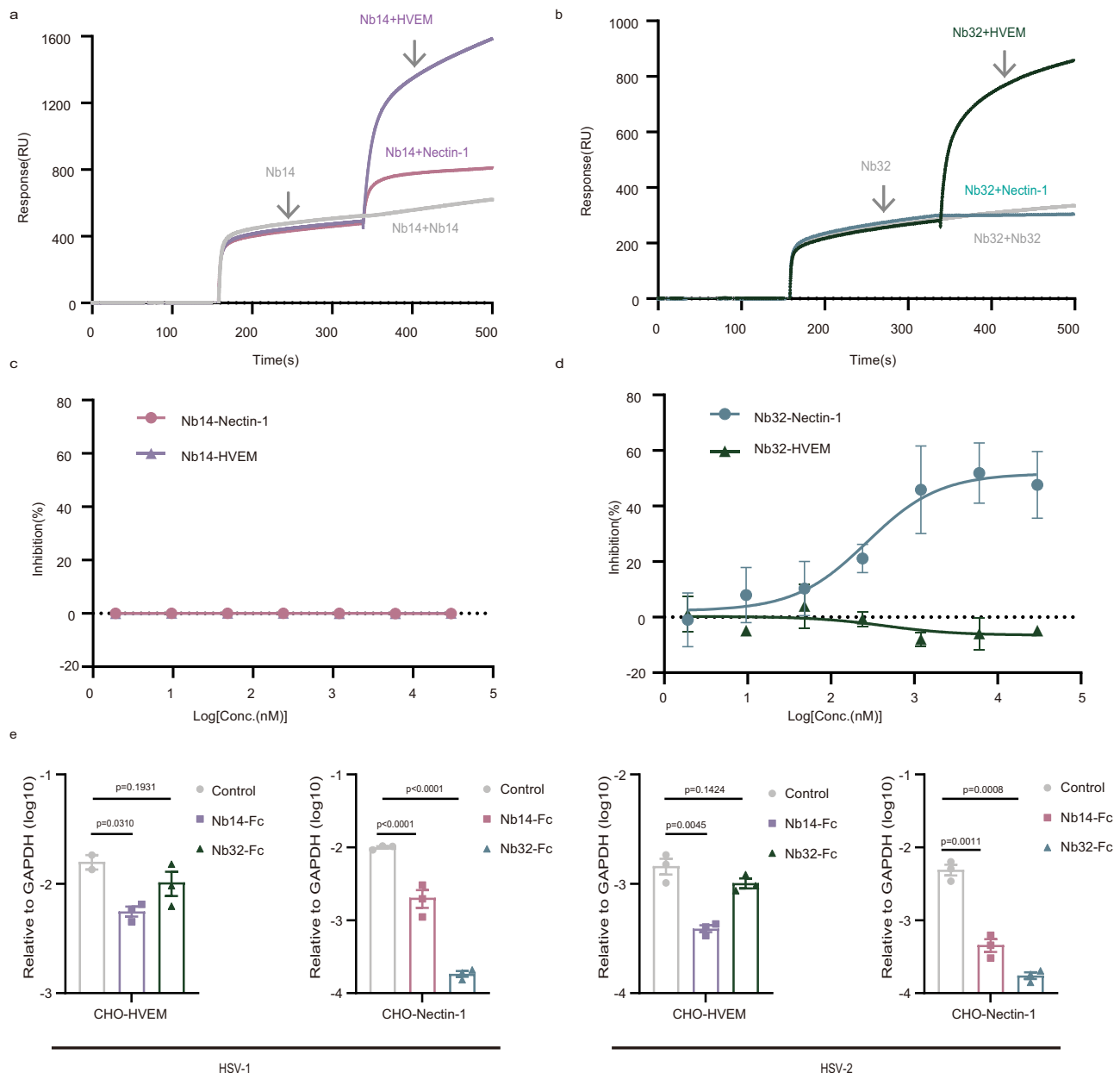
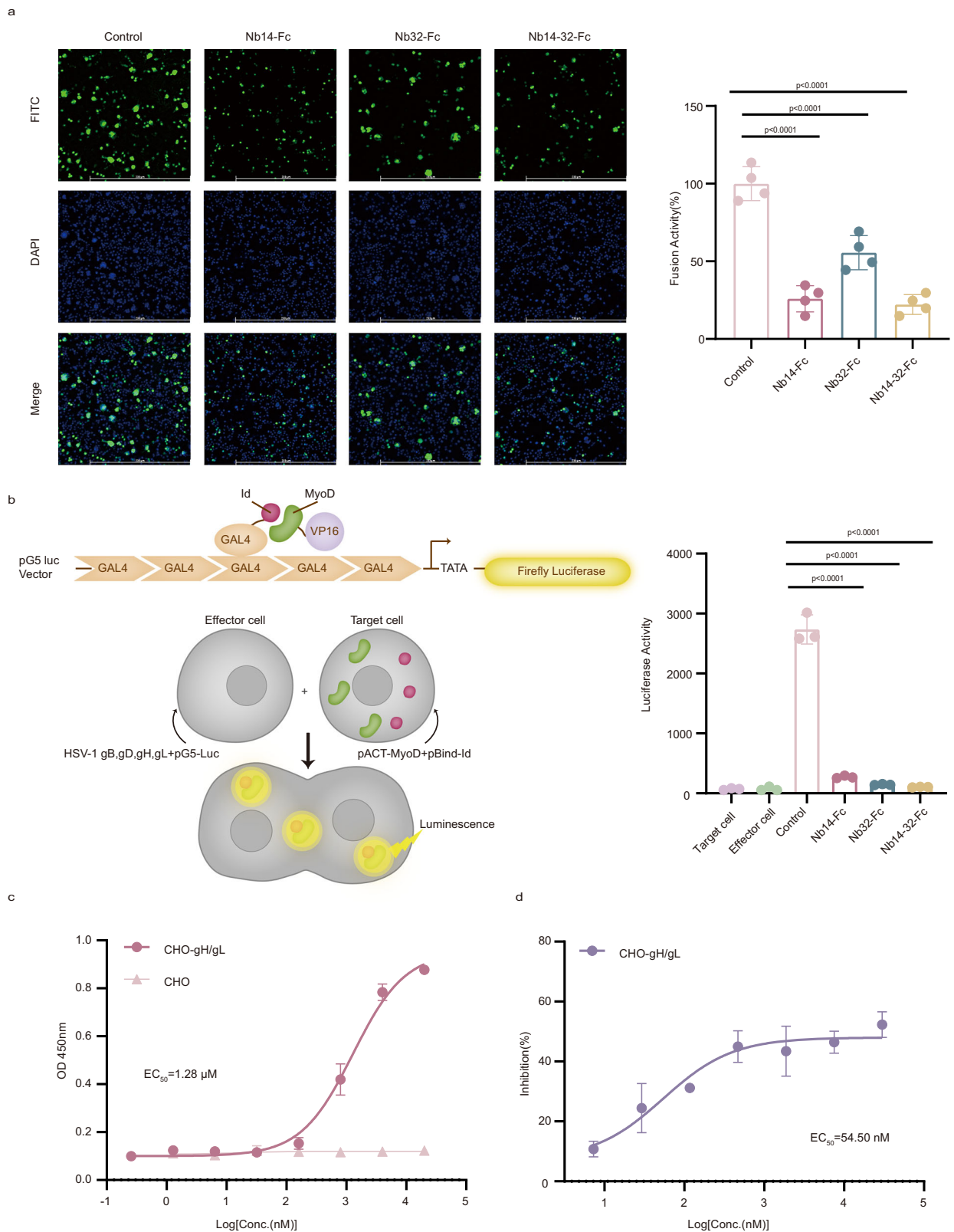


**Fig. 4 | Nb32 interferes with gD binding to its cellular receptor Nectin-1 while Nb14 acts independent of Nectin-1 or HVEM. a, b** The competitive binding kinetics of Nb14-Fc (**a**) and Nb32-Fc (**b**) with receptors were identified by surface plasmon resonance (SPR). HSV-2 gD was immobilized onto CMS sensor chip. Nbs and receptors were flowed over the chip successively. The real-time binding data are shown. **c, d** The inhibition of Nb14-Fc (**c**) and Nb32-Fc (**d**) activities were characterized by competitive ELISA, which demonstrated the ability of antibodies to inhibit the binding of HSV-2 gD to receptors expressed on CHO cells. **e** Neutralizing

potency of Nb14-Fc and Nb32-Fc characterized in CHO-Nectin-1 or CHO-HVEM cells were measured by quantitative polymerase chain reaction (qPCR). The statistical significance was determined by comparing with the control group (no antibody group) at the same infection dose using Dunnett's multiple comparison tests in a one-way ANOVA analysis, revealing a significant difference with \*\*\*\* $p < 0.0001$ , \*\*\* $p < 0.001$ , \*\* $p < 0.01$ , \* $p < 0.05$ ,  $p > 0.05$  (ns). ns, no significant. Data and error bars are mean  $\pm$  S.D,  $n = 3$  biological independent experiments in c-e. Source data are provided as a Source Data file.

kg of Nb14-Fc, Nb32-Fc or Nb14-32-Fc at 12 h after HSV-1 challenge by intraperitoneal injection (Fig. 7a). Upon HSV infection, viral loads in the brains and spinal cord were reduced by -3 logs in Nb14-32-Fc treated mice, compared to those in the control group, whereas the Nb14-Fc or Nb32-Fc treated group reduced -2 logs (Fig. 7b). Body weight loss in the control group began as early as one-day post infection (Fig. 7d). After 3–4 days, all of the mice in the control group either died of infection or reached the ethical endpoint (Fig. 7f). On the fourth day, Nb14-32-Fc still provided 100% protection while mice treated with Nb14-Fc and Nb32-Fc improved the survival rate to 75% and 62.5% compared with the control group (Fig. 7f).

To compare the therapeutic efficiency of Nb14-32-Fc with the E317 antibody, we further reduced the dose to 0.5 mg/kg and repeated the in vivo protection experiment. The results revealed that when the mice in the control group all died of infection or reached the ethical endpoint by the 4th day, at the same time, Nb14-32-Fc treatment maintained the survival rate to 80% while the mice in E317 treated group just survived 40%. Meanwhile, no significant weight loss was observed and more than one log of virus loads reduction were detected in brains and spinal cord in Nb14-32-Fc treated mice (Fig. 7c, e, g). These results demonstrated that Nb14-32-Fc had significant protective efficacy against lethal HSV-1 infection in vivo and is more effective than E317 antibody.



### Nb14-32-Fc protected mice against lethal HSV-2 vaginal infection

To assess the therapeutic efficiency of Nb-Fc antibodies against HSV-2 infection *in vivo*, we established a female BALB/c mouse model of vaginal infection with a lethal dose of HSV-2 (Fig. 8a). Medroxyprogesterone acetate was used to pretreat the mice before HSV-2 infection. The mice were treated with 1 mg/kg antibodies at 24 h after

HSV-2 challenge by intraperitoneal injection, and then repeatedly received the same treatment on day 2 and 3 after the initial treatment. In PBS-treated group, intravaginal infection of HSV-2 of mice resulted in rapid progressive disease and steady loss of body weight from day 4 post infection, with a series of abnormal symptoms such as genital lesion and behavioral disorder. In contrast, no symptoms or body weight loss were observed in the Nb14-32-Fc treated group.

**Fig. 5 | Nb14-32-Fc and its parent antibodies interfere with cell fusion and Nb14 interferes with gD binding to gH/gL.** **a** HEK-293T cells were co-transfected with glycoprotein expression plasmids (PLVX-gB-Zsgreen, PLVX-gD-Zsgreen, PLVX-gH-Zsgreen and PLVX-gL-Zsgreen) and cultured in medium containing 50 µg/ml antibodies at 37 °C for 48 h. Cells were stained with DAPI and observed under a fluorescence microscope. Scale bars, 500 µm. The relative Zsgreen area was quantified using ImageJ, with the fusion activity of the control set to 100%. **b** CHO cells which were co-transfected with glycoprotein expression plasmids and pG5-Luc were mixed with HEK-293T cells co-transfected with pACT-Myod and pBind-Id. Mixed cells were co-cultured in fresh media containing 50 µg/ml antibodies. After 48 h, cell-to-cell membrane fusion was evaluated using luciferase activity. The statistical

significance in (a) and (b) was determined by comparing with the control group (no antibody group) using Dunnett's multiple comparison tests in a one-way ANOVA analysis, revealing a significant difference with \*\*\*\* $p < 0.0001$ , \*\*\* $p < 0.001$ , \*\* $p < 0.01$ , \* $p < 0.05$ ,  $p > 0.05$ (ns). ns, no significant. Data and error bars are mean  $\pm$  S.D,  $n = 3$  biological independent experiments. **c** Multi-concentration cell-based ELISA-binding assay of HSV-2 gD towards gH/gL expressed on CHO cells. The OD<sub>450</sub> values are depicted by curves. **d** The inhibition of Nb14-Fc activities was characterized by competitive ELISA, which demonstrated the ability of Nb14-Fc to inhibit the binding of HSV-2 gD to gH/gL expressed on CHO cells. Data and error bars in (c) and (d) are mean  $\pm$  S.D,  $n = 3$  biological independent experiments. Source data are provided as a Source Data file.

More than one log of virus loads reduction in vagina and brain were detected in this group (Fig. 8b–d). All of the mice in the Nb14-32-Fc treated group survived while the mice in the control group all died of infection or reached the ethical endpoint by the 9th day (Fig. 8e). In terms of other antibodies, mice receiving Nb32-Fc also effectively protected against lethal HSV-2 infection and survived 87.5% compared to the control group. In comparison, mice receiving Nb14-Fc and E317 were less protected with the survival rate of 62.5% (Fig. 8e). To further explore the influence of HSV-2 infection on vital tissues and organs of mice, the vaginal tissues of the mice were harvested and subjected to H&E staining. Obvious pathological damage in the vaginal tissues was observed in the PBS-treated group with thinner endometrium and fewer glands. However, Nb14-32-Fc completely blocked the infection of HSV-2 in the vaginal tissues of mice and protected the mice from pathological damage caused by a lethal dose of HSV-2 (Fig. 8f). These results demonstrated that Nb14-32-Fc had significant protective efficacy against lethal HSV-2 infection in vivo and is more effective than E317 antibody.

#### Nb14-32-Fc protected mice against corneal infection caused by acyclovir-resistant strain

To evaluate the protective efficacy of antibodies against acyclovir-resistant strains in vivo, we established a male C57BL/6J mouse corneal infection model with KOS-V204G<sup>37</sup>. Mice were challenged with KOS-V204G by corneal inoculation and treated with antibodies as described in Fig. S4a. We visually examined the status of eyes and scored the severity of eye infection in all groups. Mice in the control group and acyclovir-treated group developed significant symptoms of eye infection, in contrast, KOS-V204G-caused eye symptoms were significantly alleviated in Nb14-32-Fc treated group (Fig. S4c, e). In addition, virus titers secreted from the tears decreased significantly at 3 dpi. Viral loads in the eyes and trigeminal ganglion (TG) were reduced by ~2 logs in Nb14-32-Fc treated mice at 5 dpi (Fig. S4b, d). These results demonstrated that Nb14-32-Fc had significant protective efficacy against acyclovir-resistant strain infection in vivo.

## Discussion

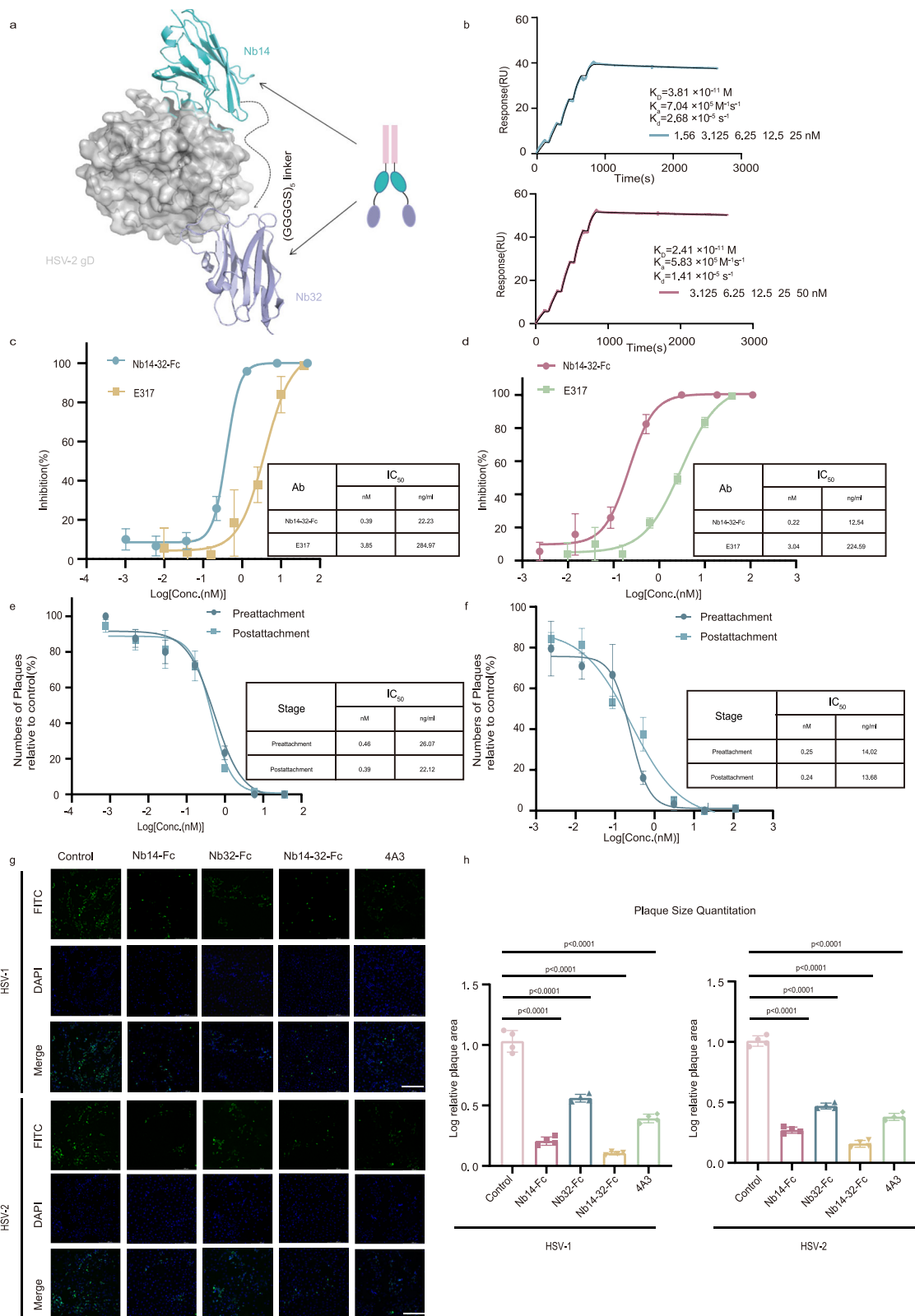
The binding of HSV gD to downstream receptors is an essential step in HSV cell entry. Hence, gD-targeting antibodies hold promise as prophylactics and therapeutics for HSV. Here, we successfully obtained two non-competing anti-gD VHH nanobodies, Nb14 and Nb32, which demonstrate potent neutralization of both HSV-1 and HSV-2 infection. Identifying the specific antibody binding epitopes can provide valuable insights into the mechanisms of virus infection, offering guidance for the rational design of vaccines. However, most known HSV gD antibody binding epitopes are identified by amino acid mutation, but lack of complex structure analysis. In consistent with our biochemical binding assays, our structural data revealed that the epitopes recognized by Nb14 and Nb32 are distinct. Nb32 is a classical nanobody that prevents the virus from invading host cells by competitively binding to gD with the receptor Nectin-1. Different

from the Nb32, our structural analysis showed that Nb14 binding epitope does not overlap with both of currently known receptors HVEM or Nectin-1 and the estimated epitopes of antibodies reported previously. Further studies indicated that Nb14 may hinder the fusion process after receptor binding mainly by interfering gD and gH/gL interactions. It is worth noting that both Nb14 and Nb32 VHH antibodies exhibited potent neutralization of HSV infection, with Nb32 being more potent than Nb14, which may be due to higher antibody affinity and different neutralization mechanisms.

Linking multiple non-competing binders to increase interacting interface is often an effective way for rational design of protein binders. We fused Nb14-Fc to Nb32 to construct a novel bispecific Nb dimer Nb14-32-Fc to further expand the antibody binding interface. We and other colleagues have successfully used such strategy in other antibody development<sup>26,27</sup>. As expected, the binding affinity, neutralizing activity and protective efficacy of Nb14-32-Fc all improved compared to the single VHH antibodies, Nb14-Fc or Nb32-Fc. Indeed, the neutralizing activity of Nb14-32-Fc in vitro is nearly 4 to 335 fold higher than that of the currently known antibodies E317, HSV8, CH42, CH43, 4A3, 2c, and HDIT102 (Table S2)<sup>16–18,38–41</sup>. In mouse models infected with common laboratory-adapted strains, administration of 1 mg/kg doses of Nb14-32-Fc protected 100% of mice against lethal doses of HSV-1/HSV-2 and its therapeutic efficacy is significantly better than that of the clinical antibody E317, HSV8, 2c and reported antibodies 4A3 and HDIT102. (Figs. 7, 8, Table S2). It is worth mentioning that in our study, we specifically established an HSV-1 brain infection model and applied it for the first time to evaluate the efficacy of neutralization antibody therapy for HSV-1 infection to simulate encephalitis. HSV-1 can be responsible for life-threatening HSV encephalitis (HSE) in human. The mortality rate of patients with HSE who do not receive antiviral treatment is 70%, with most survivors suffering from permanent neurological sequelae<sup>1,42–44</sup>. The obvious therapeutic efficacy of our bispecific antibody on HSV-1 encephalitis mice suggests that it may be a potent drug candidate for the treatment of severe herpes infection.

We further explored the neutralization mechanism of Nb14-32-Fc. Cell-to-cell spread of viruses not only accelerates viral dispersion but also has the potential to induce immune evasion and increase the risk of infection<sup>45</sup>. Notably, Nb14-32-Fc markedly inhibited cell-to-cell spread of HSV (Fig. 6g, h). Antibodies can neutralize enveloped viruses mainly by affecting viral attachment or the viral entry process of post-attachment (co-receptor binding or fusion)<sup>46</sup>. Nb14-32-Fc in this study could neutralize HSV infection at both the pre- and post-attachment stages with nearly equal efficiency. Long-lasting neutralization and effective inhibition of intercellular spread may be the main reason why bispecific nanobody exhibited significant high therapeutic efficacy in vitro and in vivo.

In conclusion, we identified two novel HSV gD-specific neutralizing Nbs termed Nb14 and Nb32, where Nb14 binds to non-classical epitopes that do not compete with conventional receptors and further engineered a novel bispecific Nb dimer, Nb14-32-Fc, which exhibited powerful antiviral ability in vitro and in vivo. Our



findings will facilitate the development of vaccine or novel therapeutic strategies against HSV.

## Methods

### Ethics statement

All work with animals was approved by the University of Science and Technology of China Laboratory Animal Management Ethics

Committee. All manipulations were strictly conducted in accordance with animal ethics guidelines. (ID: USTCACUC24120124057).

### Cells and viruses

HEK293T (ATCC, CRL-11268™), Vero E6 (ATCC, CRL-1586™) cells were cultured in Dulbecco's modified Eagle's medium (DMEM, KeyGEN) supplemented with 10% fetal bovine serum (FBS, KeyGEN) and

**Fig. 6 | Engineering of Nb-14-32-Fc with improved neutralizing potency.**

**a** Diagram showing the modification of Nb-14-32-Fc. Nb14 and Nb32 are tandemly linked with a (GGGGS)<sub>5</sub> linker and then fused with a human IgG1 Fc tag. HSV-2 gD is shown in gray surface. Nb14 and Nb32 are depicted in cartoon and highlighted in cyan and light blue, respectively. **b** The binding kinetics of Nb14-32-Fc to HSV gD were monitored by the Biacore 8 K system. The actual responses (colored lines) and the data fitted to a 1:1 binding model (black dotted lines) are shown.  $K_D$ , equilibrium dissociation constant;  $k_a$ , association constant;  $k_d$ , dissociation constant. **c, d** The neutralizing activities of Nb-14-32-Fc and E317 against HSV-1(c) and HSV-2(d). The half-maximal inhibitory concentration (IC<sub>50</sub>) values of the plaque reduction neutralization test (PRNT) were calculated by fitting the inhibition rates against antibody concentrations with a sigmoidal dose-response curve. **e, f** Comparison of the neutralization efficacy of Nb14-32-Fc when serial dilutions of the antibody were added before (pre-attachment) or after (post-attachment) HSV-1(e) and HSV-2(f)

virions interacted with Vero cells. Neutralization effects were determined after 72 h post-infection by the standard plaque assay. **g, h** Cell-to-cell spread of HSV-1 and HSV-2 in Vero cells was detected by infectious center assay. Vero cells were infected with HSV-1 and HSV-2 at an MOI of 5 in the presence of camel immune serum to neutralize any free virus released into the medium. After a total incubation of 5 h, the infected cells were detached with trypsin, plated onto uninfected Vero cells and then the antibodies were added. Cells were fixed and observed by fluorescence microscopy at 48 h post-infection. The infected cells without antibodies were used as a control. The statistical significance was determined by comparing with the control group using Dunnett's multiple comparison tests in a one-way ANOVA analysis, revealing a significant difference with \*\*\*\* $p < 0.0001$ , \*\*\* $p < 0.001$ , \*\* $p < 0.01$ , \* $p < 0.05$ ,  $p > 0.05$ (ns). ns, no significant. Scale bars, 200  $\mu$ m. Data and error bars are mean  $\pm$  S.D.,  $n = 3$  biological independent experiments in (c–h). Source data are provided as a Source Data file.

penicillin–streptomycin (Biosharp, BL505A). Expi293F (Thermo Fisher, A14528) cells were cultured in CD 293 01 medium (JSBio). CHO-K1 cells (Pricella, CL-0062) were cultured in Ham's F-12K (Pricella, PM150910) supplemented with 10% FBS(Pricella,164210-500) and penicillin–streptomycin (Biosharp, BL505A). HSV-2 (G strain) were purchased from China Center for Type Culture Collection. HSV-1-GFP (F strain) was generously provided by Zhigang Tian from the University of Science and Technology of China. HSV-1-V204G (KOS strain) was kindly provided by Dongli Pan from Zhejiang University. The titers of the viral stocks were determined by HSV plaque assay.

**Animal models**

Male C57BL/6J mice and female BALB/c mice of 6–8 weeks were purchased from GemPharmatech Co., Ltd, China. The allocation into experimental groups was random in all animal experiments. All animals were housed in specific pathogen-free (SPF) animal facilities on a 12 h light/dark cycle under ambient conditions with free access to food and water. The relative humidity was kept at 45–65%. Animal rooms and cages were kept at a temperature range of 20–24°C. Viral infection was conducted in a BSL-2 facility in accordance with the guidelines for the care and use of laboratory animals.

**Protein expression and purification**

The soluble proteins of HSV gD were prepared as previously described with some modification<sup>18</sup>. Briefly, the coding sequences for HSV-1 gD (aa1-275) and HSV-2 gD (aa1-275) were cloned into the pTT5 vector containing a C-terminal His tag (PTT5-His). Both expression vectors were transiently transfected to human HEK293F cells with polyethyleneimine (Polyscience, 23966) and the culture supernatants were collected for purification. The His-tagged gD proteins were purified using a nickel column (GE Healthcare) and eluted with 20 mM Tris-HCl, 250 mM NaCl, 400 mM imidazole pH 8.0. Protein solutions were dialyzed against 1  $\times$  PBS pH 7.5 and the concentration was measured using the spectrophotometer (Analytik Jena).

The coding sequences for Nb14, Nb32 and Nb14-32 were cloned into the pTT5 vector containing a human IgG1Fc at the C-terminus (PTT5-Fc) and expressed as a Nb-Fc fusion (termed Nb-Fc). The linker between Nb14 and Nb32 is five repeats of "GGGGS". For mAb E317 production, the genes coding heavy chain and light chain of E317 were optimized and synthesized by General Biology (Anhui) Company, and then cloned into expression vector PTT5-Fc and PTT5-His, respectively. The two plasmids were co-transfected into HEK293F cells at a DNA mass ratio of 1:1.2. The fusion proteins were all purified from cell supernatants using protein A column (Genebiol). Nb14 and Nb32 with a 6 $\times$ His-tag used for crystallization was expressed and purified in a similar manner as the above mentioned HSV gD.

**Phage display**

The phage display experiments were carried out according to the method of Ma et al.<sup>27</sup>. A male camel was immunized by 4 times with

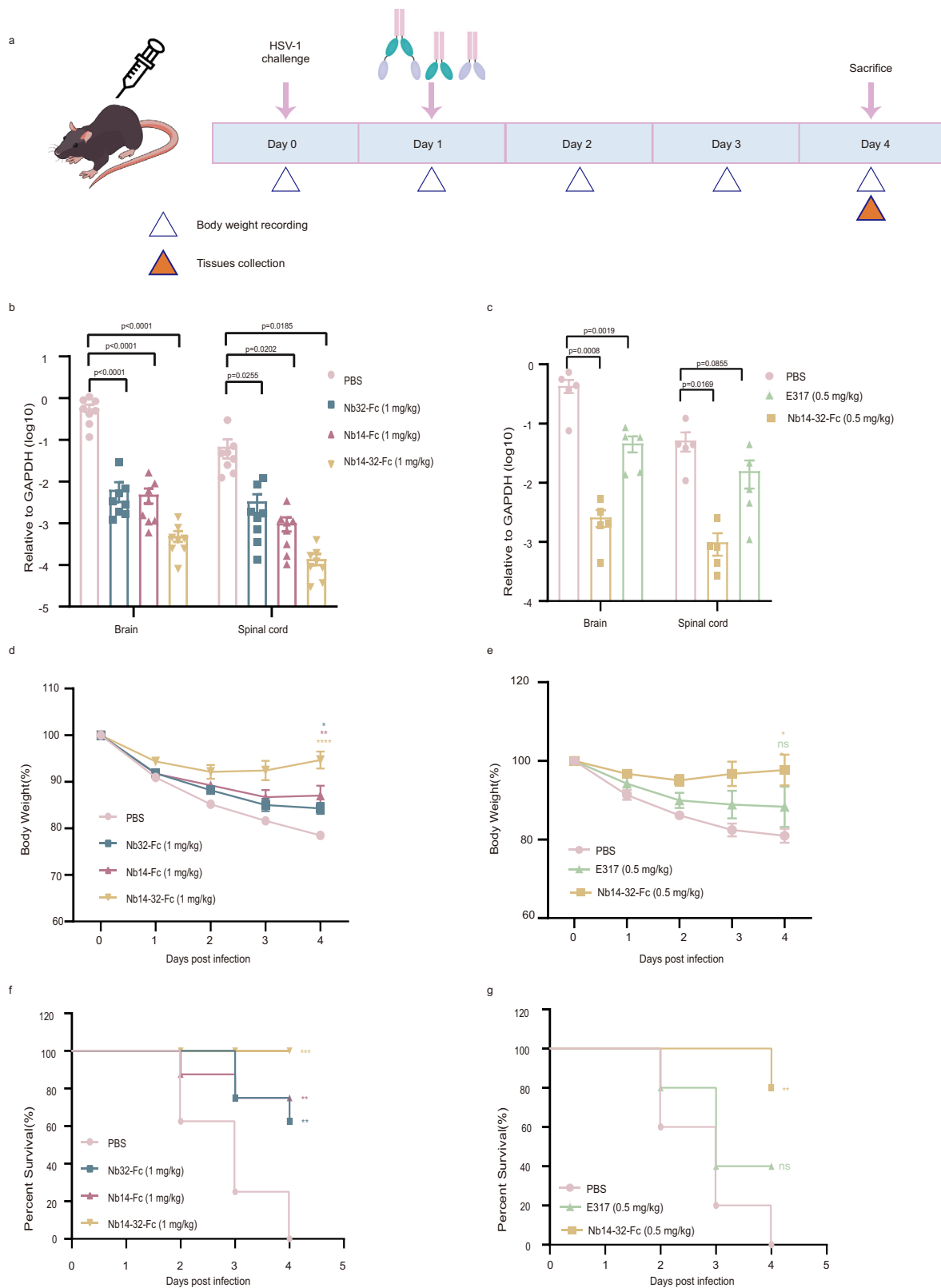
500  $\mu$ g HSV-2 gD in PBS, emulsified with an equal volume of Freund's adjuvant (Sigma Aldrich). After the final boost,  $>1 \times 10^7$  lymphocytes were isolated from peripheral blood by Ficoll (Sigma Aldrich) separation, and the total RNA was isolated using Total RNA kit (Omega Bio-Tek) according to the manufacturer's protocol. First-strand cDNA synthesis was performed using PrimeScript™ II 1st Strand cDNA Synthesis Kit and the variable domain of heavy-chain only antibody (VHH) and the phagemid pR2 were amplified by PCR. The recombinant VHH-PR2 vectors were constructed based on the Gibson assembly method and transformed into TG1 competent cells. The colonies were scraped from the plates and 200  $\mu$ L of the liquid was inoculated to amplify the library. Phage particles displaying VHH were rescued from the library using KM13 helper phage.

Immuno MaxiSorb plates (Nunc) were coated with 0.1 mL of HSV-2 gD solution (100  $\mu$ g/mL and 10  $\mu$ g/mL in the 1<sup>st</sup> and 2<sup>nd</sup> round, respectively). Control wells without antigen coating were used in parallel in every round of panning. After blocking with MPBS (PBS supplemented with 5% milk powder) for 2 h at room temperature (RT),  $1 \times 10^{11}$  PFU of library phages displaying VHH were added for the 1<sup>st</sup> round of selection. The wells were washed with PBST (PBS supplemented with 0.1% Tween 20) 20–30 times to remove the unbound phages. Bound phages were eluted by digestion with trypsin for 1 h at RT. The eluted phages were used to infect TG1 cells for titer determination and amplification. The 2<sup>nd</sup> round of panning was performed similarly except that the amount of input phage was  $1 \times 10^8$  PFU.

**Enzyme-linked immunosorbent assay (ELISA)**

To test the binding activity of Nb-Fc to HSV-1 gD or HSV-2 gD, immuno MaxiSorb plates (Nunc) were coated with HSV gD at a final concentration of 2  $\mu$ g/mL overnight at 4 °C. The plates were washed with PBST and then blocked with MPBS for 2 h at RT. Nb-Fc solutions that were serially diluted by a 1:4 ratio was added to the plates and incubated for 1 h at RT. After washing with PBST 4 times, the bound Nb-Fc was detected with a monoclonal HRP-conjugated anti-human IgG1 Fc antibody (Sino Biological, Cat#105327-MM02T-H,1:10000). For characterizing the epitope competition between the Nb14 and Nb32, 1:4 diluted Nb32 solutions (ranging from 2.5–10240 nM) were mixed with 5 nM of Nb14-Fc solutions. After incubation in HSV-2 gD coated wells and standard washing, bound Nb-Fc was detected with a monoclonal anti-IgG1 Fc-HRP antibody (Sino Biological, Cat#105327-MM02T-H,1:10000).

For cell-based ELISA of CHO-K1 cells expressing gH/gL on the surface and HSV-2 gD binding assays, CHO-K1 cells were transiently transfected with PLvx-gH-ZsGreen, PLvx-gL-ZsGreen plasmid. After protein expression for 36 h, plates were fixed for 20 min at room temperature with 1% glutaraldehyde solution. The plates were subsequently washed with PBST and blocked with 5% skim milk for 2 h. The HSV-2 gD-His solutions that were serially diluted 1:4 was added to the plates and incubated at room temperature for 1 h. After washing four times with PBST, the bound HSV-2 gD-His was detected using an



anti-his tag antibody (Sino Biological, Cat#105327-MM02T-H,1:10000). For the competitive ELISA assay to characterize the blocking activities of Nb14-Fc to gH/gL, the Nb14-Fc solution was serially diluted 1:4 with 600 nM HSV-2 gD-His solution and then added to the CHO-gH/gL coated 96-wells and incubated for 1 h. For the competitive ELISA assay to characterize the blocking activities of antibodies to receptors, the Nb14-Fc and Nb32-Fc solution were serially diluted 1:4 with 125 nM

HSV-2 gD-His solution and then added to the CHO-Nectin-1 or CHO-HVEM coated 96-wells and incubated for 1 h. After washing 4 times, bound HSV-2 gD-His was detected with anti-his tag antibody (Sino Biological, Cat#105327-MM02T-H,1:10000). After incubation for 1 h at RT, the plates were washed, 100  $\mu$ L per well of TMB (Beyotime) was added and incubated in the dark for 5 min, and 50  $\mu$ L per well of H<sub>2</sub>SO<sub>4</sub> (1 M) was added to stop the reaction. The OD<sub>450</sub> was read by a Synergy

**Fig. 7 | Nb14-32-Fc and its parent nanobodies provide therapeutic protection against intracranial infection of HSV-1 F strain in mice.** **a** Animal experiment scheme. In comparison of treatment efficacy of Nb14-32-Fc and its parent nanobodies, mice were divided into four groups ( $n = 8$  per group), including a control group administered vehicle (PBS) and three treatment groups. In comparison of treatment efficacy of Nb14-32-Fc and E317, mice were divided into three groups ( $n = 5$  per group), including a control group administered vehicle (PBS) and two treatment groups. Mice were intracranially infected with the HSV-1 F strain; 12 h later, mice were administered with antibodies or PBS via an intraperitoneal route (i.p.). The mice were then sacrificed on the 4th day of infection. **b, c** Viral RNA copies of HSV-1 in the brain and spinal cord of mice were measured with quantitative polymerase chain reaction (qPCR) on day 4 post infection. Each data point represents an individual mouse within the respective groups. **d, e** Weight loss of infected mice in the control group and treatment groups. Weight loss was

monitored daily. **d** Nb32-Fc vs PBS ( $p = 0.0359$ ), Nb14-Fc vs PBS ( $p = 0.0016$ ), Nb14-32-Fc vs PBS ( $p < 0.0001$ ) ( $n = 8$  biologically independent animals per group). **e** E317 vs PBS ( $p = 0.3367$ ), Nb14-32-Fc vs PBS ( $p = 0.0187$ ) ( $n = 5$  biologically independent animals per group). Error bars represent the mean  $\pm$  SEM. Data in **(b–e)** were analyzed by the one-way ANOVA with Dunnett's test in the comparison to PBS treated group, revealing a significant difference with \*\*\*\* $p < 0.0001$ , \*\*\* $p < 0.001$ , \*\* $p < 0.01$ , \* $p < 0.05$ ,  $p > 0.05$ (ns), ns, no significant. **f, g** Survival curves of infected mice in the control group and treatment groups. Clinical symptoms were monitored daily. Data were analyzed by the two-sided log-rank (Mantel–Cox) test. **f** Nb32-Fc vs PBS ( $p = 0.0048$ ), Nb14-Fc vs PBS ( $p = 0.0072$ ), Nb14-32-Fc vs PBS ( $p = 0.0002$ ) ( $n = 8$  biologically independent animals per group). **g** E317 vs PBS ( $p = 0.2019$ ), Nb14-32-Fc vs PBS ( $p = 0.0048$ ). ( $n = 5$  biologically independent animals per group). Source data are provided as a Source Data file.

H1 plate reader (Biotek). The data were analyzed using GraphPad Prism software.

### Surface Plasmon Resonance (SPR)

SPR measurements were performed using a Biacore 8 K system (Cytiva). Nb-Fc solutions were diluted to  $5 \mu\text{g}/\text{mL}$  with sodium acetate at pH 4.0 and immobilized on an activated Protein A chip (Cytiva). The blank channel of the chip was used as the negative control. HSV-1 gD and HSV-2 gD, which were serially diluted 1:2, were flowed over the sensor chip and the kinetics was determined by single-cycle kinetics/affinity procedure. After each cycle, the chip was regenerated with 50 mM NaOH buffer for 60 s. The sensorgrams were fitted with a 1:1 binding model using Biacore evaluation software. To determine the competition between Nbs and receptors in binding to HSV-2 gD, HSV-2 gD was diluted to a concentration of  $5 \mu\text{g}/\text{mL}$  with sodium acetate (pH 4.5) and immobilized on an activated CM5 chip (Cytiva). Nbs were injected at a concentration of 2000 nM for 180 s to achieve binding saturation, followed by HVEM or Nectin-1 or original Nbs at a concentration of 2000 nM for 180 s. A rise in signal means there is no competition between the Nbs and receptors.

### Plaque reduction neutralization test (PRNT)

Vero cells were seeded into 24-well plates and cultured overnight until the formation of monolayer cells. The Nb-Fc solutions were serially diluted in DMEM. 75 PFU of virus were incubated with antibodies at  $37^\circ\text{C}$  for 1 h and then added to Vero cells. Cells infected with virus without antibody addition were used as controls. After another 2 h of incubation at  $37^\circ\text{C}$ , the cell monolayers were overlaid with 2% methylcellulose medium and then incubated at  $37^\circ\text{C}$  for 72 h. Finally, the cells were fixed with 4% paraformaldehyde and stained with crystal violet. The plaques were manually counted using a white light transilluminator and the neutralization  $\text{IC}_{50}$  that was defined as the highest antibody concentration causing a 50% plaque reduction was calculated using GraphPad Prism software. To determine whether neutralization activities were complement-dependent, 10% guinea pig serum (Solarbio) was used as the complement source to be added into the virus-antibody mixture.

### Pre-attachment or post-attachment neutralization assay

The pre-attachment or post-attachment neutralization assays were performed as previously described<sup>39</sup>. In brief, a virus-antibody mixture was incubated for 1 h at  $4^\circ\text{C}$  before inoculation over Vero cells (pre-attachment). Prechilled Vero cells were infected with HSV at  $4^\circ\text{C}$  for 1 h before serial dilutions of antibodies were added (post-attachment). Finally, inoculated Vero cells were incubated for 2 h at  $37^\circ\text{C}$ .  $\text{IC}_{50}$  was determined after 72 h as described above PRNT.

### Infectious center assays

Infectious center assays were performed according to previously researches<sup>47</sup>. Vero cells plated in 24-well plates at 50% confluence

were exposed to HSV-1 or HSV-2 at a MOI of 5, at  $37^\circ\text{C}$  to allow entry. After 90 min of incubation, the cells were washed once with PBS and then incubated in citrate buffer (pH 3.0) for 1 min to inactivate residual virus particles. The monolayer was then washed twice with PBS to remove the citrate buffer, and the cells were placed in growth medium supplemented with camel immune serum to neutralize any extracellular virus. After a total incubation of 5 h, the infected cells were detached with trypsin-EDTA and half cells were plated onto 50% confluent monolayers of uninfected Vero cells in medium containing camel immune serum. Nb14-Fc, Nb32-Fc, Nb14-32-Fc and 4A3 ( $50 \mu\text{g}/\text{mL}$ ) were added to evaluate the effect on cell-to-cell spread. Cells were fixed with 4% paraformaldehyde after 48 h. HSV-1 infection groups were directly observed. HSV-2 infection groups were blocked with 5% BSA for 1 h and stained with the HSV-1/2 ICP5 antibody (Santa Cruz, Cat#sc-56989, 1:200 dilution) overnight at  $4^\circ\text{C}$ , and then incubated with Alexa Fluor 488 donkey anti-mouse IgG (Jackson ImmunoResearch, Cat#AB\_2340846, 1:200 dilution) before examination using a thunder DMI8 confocal microscope (Leica). Quantification of cell-to-cell spread was performed by calculating the infection area in four randomly selected regions and using image J software for analysis.

### Post-absorption virus neutralization assay

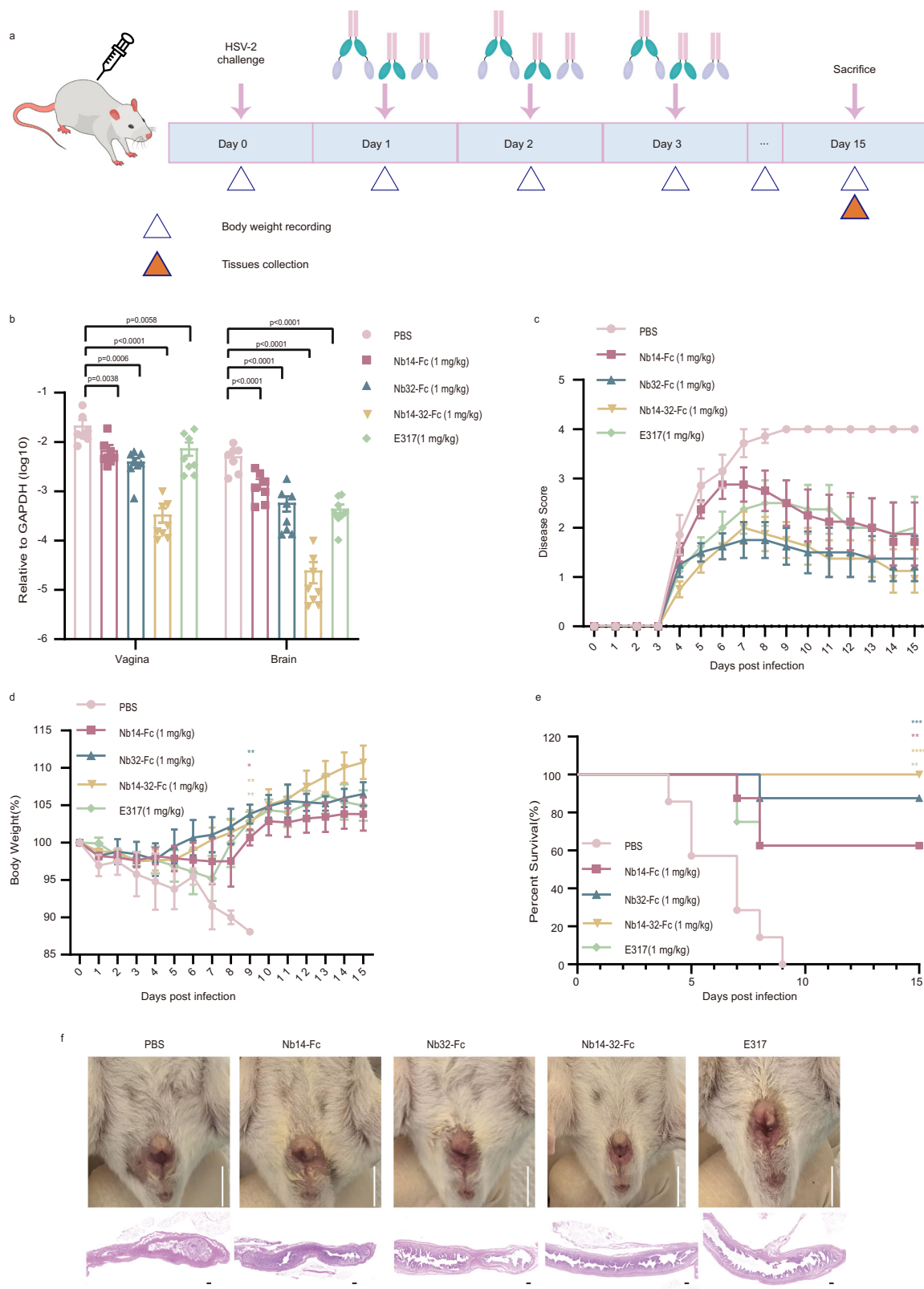
Vero cells grown to confluence in 24-well plates were incubated for 4 h at  $37^\circ\text{C}$  with 150 PFU of virus. Cell monolayers were washed twice with PBS and then incubated in citrate buffer (pH 3.0) for 1 min to inactivate residual virus particles. After twice more washing with PBS, cell monolayers were washed twice with PBS and overlaid with plaqueing medium (DMEM, 5% [wt/vol] methylcellulose, 2% FBS, and antibiotics) containing an excess of neutralizing antibodies. Plaque formation was analyzed by crystal violet staining after 48 h of incubation at  $37^\circ\text{C}$ . Twelve plaques were randomly selected for infection area analysis using image J software.

### Flow cytometry

For cell-to-cell spread assay, Vero cells were infected with the HSV-1-GFP, respectively, at an MOI of 10 for 2 h. After digestion by trypsin, half cells per samples were taken out followed by co-cultivation with uninfected cells which were labeled with CellTracker Blue fluorescence dye (MedChemexpress). Two days later, cells were washed three times with PBS and fixed with 1% paraformaldehyde. The CellTracker Blue<sup>+</sup> GFP<sup>+</sup> populations were analyzed using CytoFlex S flow cytometer (Beckman). Data were analyzed by Flowjo software.

### Crystallization and data collection

For crystallization screening, the nanobody/HSV-2 gD complex was prepared. In brief, HSV-2 gD was mixed with nanobody at a molar ratio of 1:1.2 and then incubated at  $4^\circ\text{C}$  overnight to form a complex. The mixture was further loaded on a Superdex 200 column (GE Healthcare) to remove excessive Nb. The protein complex fractions were then



pooled and concentrated to 15 mg/mL for crystallization screening. The crystallization screenings were performed using sitting-drop vapor diffusion method by mixing 0.2  $\mu$ L of protein complexes with an equal volume of reservoir solution. The crystals for the Nb14/HSV-2 gD complex were grown in the condition consisting of 0.2 M Ammonium citrate dibasic (pH 5.1) and 20% w/v Polyethylene glycol 3350. The crystals for the Nb32/HSV-2 gD complex were obtained in

conditions containing 0.1 M MES monohydrate (pH 6.0) and 14% w/v Polyethylene glycol 4000. For data collection, single crystal was flash-cooled in liquid nitrogen and sent to the Shanghai Synchrotron Radiation Facility (SSRF). X-ray diffraction data were collected at beamline BL10U2 for Nb14/HSV-2 gD at the wavelength of 0.97918  $\text{\AA}$ , and BL18U1 for Nb32/HSV-2 gD at the wavelength of 0.97853  $\text{\AA}$  at 100 K.

**Fig. 8 | Nb14-32-Fc and its parent nanobodies provide therapeutic protection against vaginal infection of HSV-2 G strain in mice.** **a** Animal experiment scheme. Mice were divided into 5 groups ( $n = 8$  per group), including a control group administered vehicle (PBS) and four treatment groups. **b** Viral RNA copies of HSV-2 in the brain and vagina of mice were measured with quantitative polymerase chain reaction (qPCR) on day 15 post infection. Each data point represents an individual mouse within the respective groups. The data ( $n = 8$  biologically independent animals per group) were subjected to one-way ANOVA with Dunnett's test in the comparison to PBS treated group. Error bars represent the mean  $\pm$  SEM, revealing a significant difference with \*\*\*\* $p < 0.0001$ , \*\*\* $p < 0.001$ , \*\* $p < 0.01$ , \* $p < 0.05$ ,  $p > 0.05$ (ns). ns, no significant. **c** Symptoms of genital disease in each group was scored daily after antibodies treatment. Error bars represent mean values with SEM ( $n = 8$  biologically independent animals per group). **d** Weight loss of infected mice in the control group and treatment groups. Weight

loss was monitored daily. Weight data ( $n = 8$  biologically independent animals per group) represent mean  $\pm$  SEM of mice remaining at each time point. The statistical significance of the 9th day was determined using Dunnett's multiple comparison tests in a one-way ANOVA analysis. \*\*\*\* $p < 0.0001$ , \*\*\* $p < 0.001$ , \*\* $p < 0.01$ , \* $p < 0.05$ . Nb32-Fc vs PBS( $p = 0.0019$ ), Nb14-Fc vs PBS( $p = 0.0132$ ), Nb14-32-Fc vs PBS( $p = 0.0036$ ), E317 vs PBS( $p = 0.0041$ ). **e** Survival curves of infected mice in the control group and treatment groups. Clinical symptoms were monitored daily. Data ( $n = 8$  biologically independent animals per group) were analyzed by the two-sided log-rank (Mantel-Cox) test. Nb32-Fc vs PBS( $p = 0.0002$ ), Nb14-Fc vs PBS( $p = 0.0039$ ), Nb14-32-Fc vs PBS( $p < 0.0001$ ), E317 vs PBS( $p = 0.0063$ ). **f** The vaginal tissues of the control and treatment groups were examined by image taken and HE staining. Scale bars of image, 1 cm; Scale bars of HE stained section, 200  $\mu$ m. Source data are provided as a Source Data file.

## Structural determination

X-ray diffraction data were processed with XDS<sup>48</sup>. Initial phases were solved by the molecular replacement method with Phaser from the CCP4i suite using HSV-2 gD (PDB ID: 4MYV) and Nb structures predicted by alphafold2 as search models<sup>49</sup>. Subsequent model building and refinement were achieved using COOT and Phenix<sup>50</sup>. All structural figures were generated with Pymol (<https://pymol.org/>). 80.52%/0.57% residues of Nb14/HSV-2 gD in the favored/disallowed region of the Ramachandran plot. 93.33%/0% residues of Nb32/HSV-2 gD in the favored/disallowed region of the Ramachandran plot.

## Virus-free fusion assay

HEK-293T cells were plated in 24-well plates, and when they reached 70%–80% confluence, the cells were co-transfected with 500 ng of PLvx-gD-ZsGreen, PLvx-gB-ZsGreen, PLvx-gH-ZsGreen, and PLvx-gL-ZsGreen and cultured in medium containing 50  $\mu$ g/ml antibodies at 37 °C for 48 h. The cells were observed under a thunder DMI8 confocal microscope (Leica), and the fusion activity was assessed by calculating the relative ZsGreen fusion area through ImageJ software.

To further verify cell-to-cell fusion, a luciferase assay was carried out. Effector CHO-K1 cells were transiently transfected with expression plasmids pLvx-gD-ZsGreen, pLvx-gB-ZsGreen, pLvx-gH-ZsGreen, pLvx-gL-ZsGreen and pGL5-Luc. Target cells (HEK-293T) were transfected with the pBind-Id and pACT-Myod plasmid. After 24 h, the effector cells were trypsinized and pre-incubated with 10  $\mu$ g Nb14-Fc, Nb32-Fc, Nb14-32-Fc at 37 °C for 1 h. Then the target cells were also trypsinized and mixed with the effector cells. After 24 h, the medium was aspirated and the cells were lysed in 100  $\mu$ l of luciferase agent (britelite plus Reporter Gene Assay System, Cat#6066761). Then, 75  $\mu$ l of cell lysate was transferred to a black-bottom assay plate and luciferase activity was read on a Synergy HI plate reader (Biotek).

## Animal study

The mouse intracranial HSV-1 F strain challenge model was established as previously described with some modification<sup>51</sup>. Eight-week-old male C57BL/6J mice were randomly divided into four groups with seven or eight mice in each group, inoculated intracranially with  $10^7$  PFU HSV-1 in a volume of 25  $\mu$ L. After 12 h, the mice were treated with 1 mg/kg dose of the Nb14-Fc, Nb32-Fc and Nb14-32-Fc by intraperitoneal injection. The control group received an equivalent volume of PBS. Mice in each group were examined daily for symptoms of encephalitis disease, body weight, and mortality.

The mouse intravaginal HSV-2 G strain challenge model was established as previously described<sup>52</sup>. To improve the susceptibility of mice to HSV-2, 6-week-old female BALB/c mice were first stimulated with medroxyprogesterone acetate (2.5 mg/mouse). After 5 days, the mice were randomly divided into four groups with seven or eight mice in each group, inoculated intravaginally with  $5 \times 10^4$  PFU HSV-2 in a volume of 50  $\mu$ L. At 24 h post-vaginal challenge, the

mice were treated daily with 1 mg/kg doses of the Nb14-Fc, Nb32-Fc and Nb14-32-Fc by intraperitoneal injection for three consecutive days. The control group received an equivalent volume of PBS. Mice in each group were monitored for 15 days and examined daily for symptoms of genital disease, body weight, and mortality. Disease score was graded on a scale of 0–4 by assigning 1 point each for erythema, exudate, hair loss, and paralysis<sup>53</sup>. At 15 days post-infection, the mice were euthanized, and vaginal tissues were harvested for histopathological analysis. Hematoxylin and eosin (HE) staining was performed on vaginal tissue sections to evaluate tissue damage. Additionally, both vaginal and brain tissues were collected for viral load analysis using qPCR.

The mouse corneal V204G infection model was established as previously described<sup>37</sup>. Six-week-old male C57BL/6J mice were anesthetized, and both corneas were scarified using a 29-gauge needle. Following this, 4  $\mu$ L of PBS containing  $2 \times 10^5$  PFU of the V204G virus was dropped onto each eye. The severity of ocular disease was monitored daily for 5 days with disease scores recorded. At 20 h post-infection, mice were treated via intraperitoneal injection with 2 mg/kg of Nb14-Fc, Nb32-Fc, or Nb14-32-Fc. The control group received an equivalent volume of PBS. For the ACV-treated mice, acyclovir (1.0 mg/ml) was placed in the drinking water 20 h after viral inoculation. The water bottles containing acyclovir were replaced daily to ensure fresh drug preparations until day 5 post-infection. On days 0 and 3 post-infection, eye swabs were collected from the mice and viral titers were determined by plaque assay. To collect the eye swabs, the mice's eyes were gently proptosed, and a sterile cotton swab was used to wipe the surface of the eye three times in a circular motion and twice across the center of the cornea in a '+' pattern. The cotton swabs were then placed in 1 mL of DMEM containing 2% FBS and 1% P/S, and stored at -80 °C until titrated by plaque assay. On day 5 post-infection, the mice were euthanized, and trigeminal ganglion (TG) and eye tissues were collected for viral load analysis by qPCR.

## Quantitative PCR

Viral RNA copies were determined by quantitative PCR (qPCR). Total RNA extraction from CHO-HVEM or CHO-Nectin-1 cells and tissues was conducted utilizing TRNzol Universal reagent (Tiangen), following the manufacturer's protocol. Real-time PCR assays were carried out employing SYBR Premix Ex Taq II (Tli RNaseH Plus) (Takara), with complementary DNA synthesis facilitated by a PrimeScript RT reagent Kit with gDNA Eraser (Takara). The viral RNA copies were normalized to the housekeeping genes (GAPDH) and expressed as  $2^{-\Delta Ct}$ . The primer sequences utilized are provided below: HSV-1-ICP0-F: CTGTGCGCTTACGTGAACAA, HSV-1-ICP0-R: CATCCAGAGGCTGTCC ACT, HSV-1-ICP27-F: CTGGCGGACATTAAGGACAT, HSV-1-ICP27-R: TCA ACTCGCAGACAGACTC, HSV-2-F: GATCTACAAGTCCCGCTCG, HSV-2-R: CACCATCCCGTTACCTTGA, GAPDH-F: TGAGGCCGGTGTGAG-TATGTCC, GAPDH-R: CCACAGTCTTCTGGTGGCAGTG

### Hematoxylin and eosin (H&E) staining

Vaginal tissues of mice were fixed in 10% formalin, embedded in paraffin, and stained with hematoxylin and eosin (H&E) according to previously described methods<sup>54</sup>. H&E staining was done by Anhui Ketu Biotechnology company as a paid service.

### Statistical analyses

All functional results were analyzed using GraphPad Prism (version 8.0.2) software, and differences were evaluated by one-way or two-way ANOVA with Dunnett's multiple comparisons test comparing to the control group (statistical comparison groups are indicated in each of the Figure legends). A *p*-value of <0.05 was considered significant, and statistical significance is reported as highly significant using \**p* < 0.05, \*\**p* < 0.01, \*\*\**p* < 0.001, \*\*\*\**p* < 0.0001.

### Reporting summary

Further information on research design is available in the Nature Portfolio Reporting Summary linked to this article.

### Data availability

Source data are provided as a Source Data file. Source data are provided with this paper. The X-ray crystal structures of Nb14-HSV-2 gD and Nb32-HSV-2 gD in this study have been deposited in the Protein Data Bank under accession codes [9ISF](#) and [9ISH](#). Other structures for analysis, including 4MYW, 1JMA and 3W9E were obtained from the PDB. All other data generated in this study are provided in the Supplementary Information/Source Data file. Source data are provided with this paper.

### References

- Piret, J. & Boivin, G. Immunomodulatory strategies in herpes simplex virus encephalitis. *Clin. Microbiol. Rev.* **33**, e00105-19 (2020).
- Rowe, A. M. et al. Herpes keratitis. *Prog. Retinal Eye Res.* **32**, 88–101 (2013).
- Feng, E., Balint, E., Vahedi, F. & Ashkar, A. A. Immunoregulatory functions of interferons during genital HSV-2 infection. *Front Immunol.* **12**, 724618 (2021).
- Arduino, P. G. & Porter, S. R. Herpes simplex virus type 1 infection: overview on relevant clinico-pathological features\*. *J. Oral. Pathol. Med.* **37**, 107–121 (2008).
- Qiao, H. et al. Herpes simplex virus type 1 infection leads to neurodevelopmental disorder-associated neuropathological changes. *PLOS Pathog.* **16**, e1008899 (2020).
- James, C. et al. Herpes simplex virus: global infection prevalence and incidence estimates, 2016. *Bull. World Health Organ* **98**, 315–329 (2020).
- Williams, E. J. et al. Viral infections: contributions to late fetal death, stillbirth, and infant death. *J. Pediatrics* **163**, 424–428 (2013).
- Slutsker, J. S. & Schillinger, J. A. Assessing the burden of infant deaths due to herpes simplex virus, human immunodeficiency virus, and congenital syphilis: united states, 1995 to 2017. *Sex. Transm. Dis.* **48**, S4–s10 (2021).
- Schiffer, J. T. & Gottlieb, S. L. Biologic interactions between HSV-2 and HIV-1 and possible implications for HSV vaccine development. *Vaccine* **37**, 7363–7371 (2019).
- Aebi-Popp, K., Bailey, H., Malyuta, R., Volokha, A. & Thorne, C. High prevalence of herpes simplex virus (HSV)- type 2 co-infection among HIV-positive women in Ukraine, but no increased HIV mother-to-child transmission risk. *BMC Pregnancy Childbirth* **16**, 94 (2016).
- Tayyar, R. & Ho, D. Herpes simplex virus and varicella zoster virus infections in cancer patients. *Viruses* **15**, 439 (2023).
- Poole, C. L. & Kimberlin, D. W. Antiviral approaches for the treatment of herpes simplex virus infections in newborn infants. *Annu Rev. Virol.* **5**, 407–425 (2018).
- Kimberlin David, W. et al. Oral acyclovir suppression and neurodevelopment after neonatal herpes. *N. Engl. J. Med.* **365**, 1284–1292 (2004).
- Schalkwijk, H. H., Snoeck, R. & Andrei, G. Acyclovir resistance in herpes simplex viruses: prevalence and therapeutic alternatives. *Biochem. Pharmacol.* **206**, 115322 (2022).
- Kłysik, K., Pietraszek, A., Karewicz, A. & Nowakowska, M. Acyclovir in the treatment of herpes viruses—a review. *Curr. Med. Chem.* **27**, 4118–4137 (2020).
- Sanna, P. P. et al. Protection of nude mice by passive immunization with a type-common human recombinant monoclonal antibody against HSV. *Virology* **215**, 101–106 (1996).
- Wang, K. et al. Monoclonal antibodies, derived from humans vaccinated with the RV144 HIV vaccine containing the HVEM binding domain of herpes simplex virus (HSV) glycoprotein D, neutralize HSV infection, mediate antibody-dependent cellular cytotoxicity, and protect mice from ocular challenge with HSV-1. *J. Virol.* **91**, e00411-17 (2017).
- Lee, C.-C. et al. Structural basis for the antibody neutralization of Herpes simplex virus. *Acta Crystallogr. Sect. D.* **69**, 1935–1945 (2013).
- Krawczyk, A. et al. Overcoming drug-resistant herpes simplex virus (HSV) infection by a humanized antibody. *Proc. Natl Acad. Sci. USA* **110**, 6760–6765 (2013).
- Cairns Tina, M. et al. Localization of the interaction site of herpes simplex virus glycoprotein D (gD) on the membrane fusion regulator, gH/gL. *J. Virol.* **94**, e00983-20 (2020).
- Wu, Y., Jiang, S. & Ying, T. Single-domain antibodies as therapeutics against human viral diseases. *Front Immunol.* **8**, 1802 (2017).
- Fotouhi, F., Soleimanzahi, H., Roostaei, M. H. & Dalimi Asl, A. Expression of the herpes simplex virus type 2 glycoprotein D in baculovirus expression system and evaluation of its immunogenicity in guinea pigs. *Iran. Biomed. J.* **12**, 59–66 (2008).
- Awasthi, S. et al. Protection provided by a herpes simplex virus 2 (HSV-2) glycoprotein C and D subunit antigen vaccine against genital HSV-2 infection in HSV-1-seropositive guinea pigs. *J. Virol.* **88**, 2000–2010 (2014).
- Yang, J. et al. Development of a bispecific nanobody conjugate broadly neutralizes diverse SARS-CoV-2 variants and structural basis for its broad neutralization. *PLOS Pathog.* **19**, e1011804 (2023).
- De Meyer, T., Muyldermans, S. & Depicker, A. Nanobody-based products as research and diagnostic tools. *Trends Biotechnol.* **32**, 263–270 (2014).
- Ma, H. et al. A bispecific nanobody dimer broadly neutralizes SARS-CoV-1 & 2 variants of concern and offers substantial protection against Omicron via low-dose intranasal administration. *Cell Discov.* **8**, 132 (2022).
- Ma, H. et al. Hetero-bivalent nanobodies provide broad-spectrum protection against SARS-CoV-2 variants of concern including Omicron. *Cell Res.* **32**, 831–842 (2022).
- Carfi, A. et al. Herpes simplex virus glycoprotein D bound to the human receptor HveA. *Mol. Cell* **8**, 169–179 (2001).
- Connolly, S. A. et al. Potential nectin-1 binding site on herpes simplex virus glycoprotein D. *J. Virol.* **79**, 1282–1295 (2005).
- Di Giovine, P. et al. Structure of herpes simplex virus glycoprotein D bound to the human receptor nectin-1. *PLOS Pathog.* **7**, e1002277 (2011).
- Lu, G. et al. Crystal structure of herpes simplex virus 2 gD bound to nectin-1 reveals a conserved mode of receptor recognition. *J. Virol.* **88**, 13678–13688 (2014).
- Atanasiu, D., Saw, W. T., Cohen, G. H. & Eisenberg, R. J. Cascade of events governing cell-cell fusion induced by herpes simplex virus glycoproteins gD, gH/gL, and gB. *J. Virol.* **84**, 12292–12299 (2010).
- Fontana, J. et al. The fusion loops of the initial prefusion conformation of herpes simplex virus 1 fusion protein point toward the membrane. *mBio* **8**, e01268-17 (2017).

34. Atanasiu, D. et al. Using antibodies and mutants to localize the presumptive gH/gL binding site on herpes simplex virus gD. *J. Virol.* **92**, e01694-18 (2018).
35. Backes, I. M. et al. Maternally transferred mAbs protect neonatal mice from HSV-induced mortality and morbidity. *J. Exp. Med.* **219**, e20220110 (2022).
36. Sattentau, Q. Avoiding the void: cell-to-cell spread of human viruses. *Nat. Rev. Microbiol.* **6**, 815–826 (2008).
37. Wang, S., Hou, F., Yao, Y. F. & Pan, D. Efficient establishment of reactivatable latency by an acyclovir-resistant herpes simplex virus 1 thymidine kinase substitution mutant with reduced neuronal replication. *Virology* **556**, 140–148 (2021).
38. Tian, R. et al. A potent neutralizing and protective antibody against a conserved continuous epitope on HSV glycoprotein D. *Antivir. Res.* **201**, 105298 (2022).
39. Krawczyk, A. et al. Impact of valency of a glycoprotein B-specific monoclonal antibody on neutralization of herpes simplex virus. *J. Virol.* **85**, 1793–1803 (2011).
40. Burioni, R., Williamson, R. A., Sanna, P. P., Bloom, F. E. & Burton, D. R. Recombinant human Fab to glycoprotein D neutralizes infectivity and prevents cell-to-cell transmission of herpes simplex viruses 1 and 2 in vitro. *Proc. Natl Acad. Sci. USA* **91**, 355–359 (1994).
41. Seyfizadeh, N. et al. Development of a highly effective combination monoclonal antibody therapy against Herpes simplex virus. *J. Biomed. Sci.* **31**, 56 (2024).
42. Aurelius, E., Johansson, B., Sköldenberg, B. & Forsgren, M. Encephalitis in immunocompetent patients due to herpes simplex virus type 1 or 2 as determined by type-specific polymerase chain reaction and antibody assays of cerebrospinal fluid. *J. Med. Virol.* **39**, 179–186 (1993).
43. Raschilas, F. et al. Outcome of and prognostic factors for herpes simplex encephalitis in adult patients: results of a multicenter study. *Clin. Infect. Dis.* **35**, 254–260 (2002).
44. Jouan, Y. et al. Long-term outcome of severe herpes simplex encephalitis: a population-based observational study. *Crit. Care* **19**, 345 (2015).
45. Martin, N. & Sattentau, Q. Cell-to-cell HIV-1 spread and its implications for immune evasion. *Curr. Opin. HIV AIDS* **4**, 143–149 (2009).
46. Henrich, T. J. & Kuritzkes, D. R. HIV-1 entry inhibitors: recent development and clinical use. *Curr. Opin. Virol.* **3**, 51–57 (2013).
47. Jenssen, H., Sandvik, K., Andersen, J. H., Hancock, R. E. & Gutteberg, T. J. Inhibition of HSV cell-to-cell spread by lactoferrin and lactoferricin. *Antivir. Res.* **79**, 192–198 (2008).
48. Kabsch, W. XDS. *Acta Crystallogr. Sect. D.* **66**, 125–132 (2010).
49. McCoy, A. J. et al. Phaser crystallographic software. *J. Appl. Crystallogr.* **40**, 658–674 (2007).
50. Adams, P. D. et al. PHENIX: a comprehensive python-based system for macromolecular structure solution. *Acta Crystallogr. Sect. D.* **66**, 213–221 (2010).
51. Kollias, C. M., Huneke, R. B., Wigdahl, B. & Jennings, S. R. Animal models of herpes simplex virus immunity and pathogenesis. *J. NeuroVirol.* **21**, 8–23 (2015).
52. Ceña-Diez, R. et al. Prevention of vaginal and rectal herpes simplex virus type 2 transmission in mice: mechanism of antiviral action. *Int. J. Nanomed.* **11**, 2147–2162 (2016).
53. Du, R. et al. A novel glycoprotein D-specific monoclonal antibody neutralizes herpes simplex virus. *Antivir. Res.* **147**, 131–141 (2017).
54. Luo, Y. et al. Development of an HSV-1 neutralization test with a glycoprotein D specific antibody for measurement of neutralizing antibody titer in human sera. *Virol. J.* **13**, 44 (2016).

## Acknowledgements

We thank Feng Zhu from USTC for the management of the BSL-2 facility. We also thank the staff at the BL02U1 and BL18U1 beamline at SSRF for the assistance during X-ray data collection. This study was supported by the National Key Research and Development Program of China (Grants No. 2022YFC2304102, 2022YFC2303300), the Strategic Priority Research Program of the Chinese Academy of Sciences (Grant No. XDB0490000, XDB0940301), the National Natural Science Foundation of China (Grant No. 82272301, 82341121), Anhui Provincial Key Research and Development Project (Grant No. 2022i01020025), USTC Research Funds of the Double First-Class Initiative (YD9100002056), the Clinical Key Specialty Construction Project of Anhui Province.

## Author contributions

J.H., H.Y.T., S.Z. and T.C.J. conceptualized and designed the study. J.H., H.Y.T., M.H.W., S.S.D., M.Y.L., P.Y.Z., A.M.W., M.G., J.W., J.Y.L., H.W.Q., C.B.Y., Z.L.Z. and C.L.H. performed experiments. J.H., H.Y.T. and M.H.W. analyzed data. D.L.P., H.L.H., C.H.H. and Y.H.S. provided resources. T.C.J. acquired funding. J.H. and H.Y.T. wrote the paper. J.H., H.Y.T., S.Z. and T.C.J. revised the manuscript.

## Competing interests

The authors declare no competing interests.

## Additional information

**Supplementary information** The online version contains supplementary material available at <https://doi.org/10.1038/s41467-025-58669-7>.

**Correspondence** and requests for materials should be addressed to Shu Zhu or Tengchuan Jin.

**Peer review information** *Nature Communications* thanks Matthew Reeves and the other, anonymous, reviewer(s) for their contribution to the peer review of this work. A peer review file is available.

**Reprints and permissions information** is available at <http://www.nature.com/reprints>

**Publisher's note** Springer Nature remains neutral with regard to jurisdictional claims in published maps and institutional affiliations.

**Open Access** This article is licensed under a Creative Commons Attribution-NonCommercial-NoDerivatives 4.0 International License, which permits any non-commercial use, sharing, distribution and reproduction in any medium or format, as long as you give appropriate credit to the original author(s) and the source, provide a link to the Creative Commons licence, and indicate if you modified the licensed material. You do not have permission under this licence to share adapted material derived from this article or parts of it. The images or other third party material in this article are included in the article's Creative Commons licence, unless indicated otherwise in a credit line to the material. If material is not included in the article's Creative Commons licence and your intended use is not permitted by statutory regulation or exceeds the permitted use, you will need to obtain permission directly from the copyright holder. To view a copy of this licence, visit <http://creativecommons.org/licenses/by-nc-nd/4.0/>.

© The Author(s) 2025